Characterization of native reversible self-association of a monoclonal antibody mediated by Fab-Fab interaction

Gentiluomo, Lorenzo; Roessner, Dierk; Streicher, Werner; Mahapatra, Sujata; Harris, Pernille; Frieß, Wolfgang

Published in:
Journal of Pharmaceutical Sciences

Link to article, DOI:
10.1016/j.xphs.2019.09.021

Publication date:
2020

Document Version
Peer reviewed version

Characterization of native reversible self-association of a monoclonal antibody mediated by Fab-Fab interaction

Lorenzo Gentiluomo[1,2], Dierk Roessner[1], Werner Streicher,[3] Sujata Mahapatra, [3] Pernille Harris,[4] Wolfgang Frieß[2]

[1] Wyatt Technology Europe GmbH, Hochstrasse 18, 56307 Dernbach, Germany

[2] Ludwig-Maximilians-Universitaet Muenchen, Department of Pharmacy, Pharmaceutical Technology and Biopharmaceutics, Butenandtstrasse 5, 81377 Munich, Germany

[3] Novozymes A/S, Krogshoejvej 36, 2880, Bagsvaerd, Denmark

[4] Technical University of Denmark, Department of Chemistry, Kemitorvet 207, 2800 Kongens Lyngby, Denmark

lorenzo.gentiluomo@wyatt.eu

1 ABSTRACT

The native reversible self-association of monoclonal antibodies has been associated with high viscosity, liquid-liquid and liquid-solid phase separation. We investigated the native reversible self-association of an IgG1, which exerts this association even at low protein concentrations, in detail to gain further understanding of this phenomenon by extensive characterization of the association as a function of multiple factors, namely pH, temperature, salt concentration and protein concentration. The nature of the self-association of the full-length IgG1 as well as the corresponding Fab and Fc fragment was studied by viz. SEC-MALS, DLS, SLS, AUC, SAXS, AF4-MALS and intrinsic fluorescence. We rationalized the self-association as a combination of hydrophobic and electrostatic interactions driven by the Fab fragments. Finally, we investigated the long-term stability of the IgG1 molecule.

2 INTRODUCTION

Humanized monoclonal antibodies (mAbs) have become major biopharmaceutical products in the last decades for the treatment of cancer and autoimmune diseases,[1–3] with over 50 of such molecules

approved for therapeutic use.[4] The development of therapeutic antibodies is not straightforward, because, like other proteins, they are prone to physical instabilities and chemical degradation that need to be overcome.[5] Among these degradation pathways, protein aggregation presents one of the most common and troubling challenges. It has been shown that aggregates have reduced activity and potential for greater immunogenicity. [6–8] Moreover, it has been proven that non-native protein aggregation is at least partially the cause of several diseases, [9] among which there are Alzheimer's disease, Parkinson disease, prion diseases, Huntington's disease, Down's syndrome, cataract, and sickle cell disease. Due to this prevalence in pathology and therapeutic protein manufacturing, the study of the kinetics and mechanisms of protein aggregation is vital to future treatments. The critical review by Roberts[10] presents an excellent resource on the detailed steps of protein aggregation. In this study, a clear distinction is delineated between non-native and native protein aggregation. Native self-association have been investigated in several studies[11–13] and hydrophobic intermolecular interactions are considered to be the main driver.[14] Native reversible self-association has been associated with unusually high viscosity of concentrated mAb solutions in low ionic strength buffers which is one of the greatest challenge when developing protein formulations at higher concentrations.[11,15] It has been shown that the self-association of human myeloma protein causes the increase in viscosity through a combination of hydrophobic interactions.[16] The self-association of monoclonal serum immunoglobulins has been connected with hyperviscosity syndromes.[17–19] However, there are limited numbers of analytical methods that provide information at high protein concentrations.[20–22] This hampers an in depth characterization of the association. In this study we characterized and rationalized the behavior of an IgG1, PPI-1, which shows native reversible self-association at low ionic strength. PPI-1 exerts this association even at low protein concentrations, which allowed us to apply an extended analytical toolbox. We investigated how pH, salt concentration, protein concentration and temperature impact the degree of oligomerization. Additionally, PPI-1 was digested into its Fab and Fc fragments, to identify which regions of the mAb are involved in the oligomer formation. Previous studies have found the origin of native self-association has been localized in either the Fab and the Fc fragments.[11,12] Accelerated and long term stability studies were executed to understand the impact of the native reversible self-association on protein aggregation upon storage. Thus, this study on native reversible self-association leads to a better understanding of the underlying mechanism that helps to design antibodies that are less prone to association.[23]

3 MATERIAL AND METHODS

3.1 Sample preparation

The behavior of one IgG1, namely PPI-1, provided by the PIPPI consortium (http://www.pippi.kemi.dtu.dk) was characterized. PPI-1 was dialyzed using 10 kDa Slide-A-Lyzer™ cassettes (Thermo Fisher Scientific, Waltham, USA) into 10 mM histidine buffer pH 6.0 to obtain a 35 mg/ml solution. Then, PPI-1 was dialyzed into 10mM histidine buffer pH 5.0, 5.5, 6.5, 7.0, 7.5. NaCl stock solution in the respective buffer was added to reach 0, 70 or 140 mM. Protein concentration was measured on a Nanodrop 2000 (Thermo Fisher Scientific, Waltham, USA) using the extinction coefficient calculated from the primary sequence. All chemicals were of analytical grade and were purchased from Sigma Aldrich (Steinheim, Germany) or VWR International (Darmstadt, Germany). Highly purified water (HPW, Purelab Plus, USF Elga, Germany) was used for the preparation of all buffers. Finally, the formulations were sterile filtered with a low protein binding Millex® 0.22 µm filter (Merk Millipore, Burlington, USA).

3.2 Preparation and purification of Fab and Fc Fragments

Immobilized Papain (Thermo Fisher Scientific, Waltham, USA) was used to digest PPI-1 into its Fab and Fc fragments. PPI-1 at 20 mg/mL was pipetted into 15 mL glass vial, the vial capped with the resin separator provided with the kit to remove all the air-liquid interface. The vial was gently rotated by a Sunlab rotator SU1100 for 5 h at 37 °C. An ÄKTA purifier 10 (GE Healthcare, Uppsala, Sweden) equipped with a Pierce Protein A chromatography cartridge (Thermo Fisher Scientific, Waltham, USA) (column volume, CV = 5 ml) was used to separate Fc (and undigested mAb) from the Fab fragments. The binding buffer was composed of 100 mM sodium phosphate with 150 mM NaCl at pH 7.2. The column was equilibrated with 2 column volumes (CV) of binding buffer with a flow of 2 ml/min. Fractions were collected in 15-ml PP tubes using a Frac 920 fraction collector (GE Healthcare, Uppsala, Sweden) capturing any unbound species e.g. Fab. The elution buffer was kept at 100 % over 7 CV. The eluting protein was collected in 15-ml PP tubes using the fraction collector, and was immediately neutralized with a 1 M sodium phosphate buffer pH 8.5 to result in approx. 175 mM sodium phosphate buffer at pH 6.5. Ultrafiltration was performed using Vivaspin® tubes with a 10 kDa MWCO PES membrane (Sartorius Stedim Biotech, Göttingen, Germany). Success of the purification was monitored by HP-SEC (see 3.4). Finally, different formulations of Fab and Fc were prepared as described for the mAb in 3.1.

3.3 Long term stability study

0.2 mL of each protein solution was aliquoted at a concentration of 1 mg/mL and filtered through a 0.22 um Miller® GV filter (Merck, Millipore, USA) under a laminar flow hood into 0.5 mL sterile non-coated PP Eppendorf tubes. The samples were incubated at 4, 25, and 40 °C for 6 months.

3.4 Size exclusion chromatography coupled with multi-angle light scattering

Samples were investigated using size exclusion chromatography combined with multi-angle light scattering (SEC–MALS). The system consisted of a Vanquish HorizonTM UPLC with a variable wavelength UV detector operated at 280 nm (Thermo Fischer Scientific, Waltham, USA). The temperature controlled autosampler was kept at 4°C. The separation was performed with a Superdex 200 increased 10/30 GL column. Concentration was determined immediately after the column by a UV detector at 280 nm which was followed by a static light scattering apparatus, a TREOS II detector (Wyatt Technology, Santa Barbara, USA) followed by additional concentration verification by a differential refractive index detector (Optilab T-rEX, Wyatt Technology, Santa Barbara, USA). Data collection and processing were performed using the ASTRA software V7.2 (Wyatt Technology, Santa Barbara, USA). The mobile phase consisted of 38 mM NaH_2PO_4, 12 mM Na_2HPO_4, 150 mM NaCl and 200 ppm NaN_3 at pH 7.4 and was filtered through Durapore VVPP 0.1 µm membrane filters (Millipore Corporation, Billerica, USA). The samples were injected at a volume of 25 or 50 µL.

3.5 Asymmetric flow field flow fractionation coupled with multi-angle light scattering

Asymmetric flow field flow fractionation coupled with multi-angle light scattering (AF4–MALS) was used to study PPI-1 oligomers using the respective sample formulations as carrier. The system consisted of a pump (Agilent 1260 Infinity II, Santa Clara, USA) with an online degasser, and a temperature controlled autosampler kept at 4°C. The separation was performed with an AF4 system (ECLIPSE, Wyatt Technology Corporation, Santa Barbara, USA) using a short channel with 490 µm spacer and a pre-cut regenerated cellulose membrane with 10 kDa cut-off (Wyatt Technology, Santa Barbara, USA). A focus flow of 1.5 mL/min was applied for 2 minutes prior to injection. The samples were injected with a flow of 0.2 mL/ min maintaining the focus flow. Then the samples were focused at 1.5 mL/min for 5 min. A constant detector flow of 1 mL/min was used during the separation process, which included three stages: (1) 3 mL/min cross flow, hold constant for 20 min; (2) linear ramped flow from 3 to 0.1 mL/min in 10 min; and (3) 0.0 mL/min flow, hold constant for 5 min. A TREOS II MALS detector (Wyatt Technology, Santa Barbara, USA), a variable wavelength detector operated at 280 nm (Agilent 1260 Infinity II) and a differential refractive index detector, Optilab T-rEX (Wyatt Technology, Santa Barbara, USA) were connected to the system. Data collection and processing were performed using the ASTRA software, V 7.2 (Wyatt Technology Corporation). The respective formulation of the sample (e.g. His 10 mM at pH 5)

filtered through Durapore VVPP 0.1 µm membrane filters (Millipore Corporation, Billerica, USA) was used as aqueous mobile phase.

3.6 Dynamic and static light scattering

High throughput dynamic and static light scattering was conducted on a DynaPro® III Plate Reader (Wyatt Technology, Santa Barbara, USA) to obtain the hydrodynamic radius, R_h, and the molecular weight, M_w. 4 µL per well of each sample, filtered using a Millex® 0.22 µm filter (Merk Millipore, USA), were pipetted in triplicates into Aurora 1536 Lobase Assay Plates (Aurora Microplates, Whitefish, USA). Wells were sealed with silicone oil and then centrifuged at 2000 rpm for 1 minute. Data were processed by the Dynamics software V 7.8 (Wyatt Technology, Santa Barbara, USA). To calculate the M_w the plate was calibrated with Dextran 35-45 kDa (Sigma Aldrich; USA, Lot number: SLBQ5973V),. Composition gradient MALS (CG-MALS) and DLS (CG-DLS) were used to determine k_D using at least ten different concentrations (from 1 to 10 mg/mL) in triplicate. The samples were and equilibrated at 25 °C for 10 minutes in the Plate reader. Temperature ramps were determined at 1 mg/mL. Temperature of aggregation, $T_{agg,}$ was processed by the DYNAMICS software V7.8 onset algorithm from the increase in the total scattering intensity.

Detailed static and dynamic light scattering studies were conducted on a DynaPro® Nanostar (Wyatt Technology, Santa Barbara, USA). 2 µL of sample were pipetted into a quartz cuvette and sealed silicone oil. Measurements were conducted in triplicate.

3.7 Differential scanning fluorimetry

Samples containing 1 mg/mL protein were filled in nanoDSF capillaries and analyzed using the Prometheus NT.48 (NanoTemper Technologies, Munich, Germany). A temperature ramp of 1°C/min from 20 to 95°C was applied. The fluorescence intensity ratio (F350/F330) was plotted against the temperature, and the first apparent melting temperature (T_m) was derived from the maximum of the first derivative using the PR Control software V1.12 (NanoTemper Technologies, Munich, Germany). All measurements were performed in triplicate.

3.8 Analytical ultracentrifugation

Sedimentation velocity experiments were conducted in a Beckman XLI ultracentrifuge (Beckman Coulter Inc, Palo Alto, CA) at 40,000 rpm at 20°C using the charcoal-filled Epon 12-mm double-sector

centerpieces. The moving boundary was monitored by repetitive radial scanning at a constant step size of 0.003 cm at 280 nm using a UV absorption optical system. Sedimentation velocity data were analyzed and simulation data were created using the software program SEDFIT (National Institutes of Health, Bethesda, MD)[24] to generate the sedimentation coefficient distribution of protein samples.

3.9 Small angle X-ray Scattering (SAXS)

35 mg/mL of PPI-1 in 10 mM histidine buffer at pH 5.0, 5.5, 6.0 and 6.5 without salt was dialyzed over three shifts. The dialysate from the final buffer exchange was sterile filtered using a 0.22 um Miller® GV filter (Merck, Millipore, USA) and used for sample dilution and buffer measurements. SAXS experiments were performed at the ESRF synchrotron, BM29 bioSAXS beamline at Grenoble, France. Measurements of pure water were used to get the data on an absolute scale. Buffers were measured both before and after each sample and averaged before subtraction. A concentration range from 0.5mg/ml – 17mg/ml was measured for each formulation. Data collection parameters are listed in **Table SI 1**. Calibrations and corrections of SAXS data collected at ESRF were carried out by an automated pipeline.[25] Buffer averaging and subsequent subtraction prior to data analyses were performed in Primus.[26] The ATSAS program package version 2.8.4[27] was used for further data analysis. Primus was also used to perform Guinier region analysis and GNOM[28] was used for pair distribution, $p(r)$, analysis. The intensity, $I(q)$, is measured as a function of scattering vector $q = 4\pi\, sin\theta/\lambda$, where λ is the wavelength, and 2θ the scattering angle. Molecular weight calculations were performed using $M_w = [N_A I(0)/c]/\Delta\rho_M^2$ where N_A is Avogadro constant, $I(0)/c$ is concentration normalized forward scattering and $\Delta\rho_M$ is the scattering contrast per mass. $\Delta\rho_M$ was calculated using proteins average partial specific volume, $0.7425\ \mathrm{cm^3 g^{-1}}$.[29]

3.10 Reversed-Phase Ultra-High-Performance liquid chromatography (RP-UPLC)

Reversed phase chromatography was conducted on an ACQUITY UPLC H-Class system (Waters, UK) equipped with a quaternary pump, an autosampler, and UV detector. The separation was performed with a Acquity BEH-300 C4 (Waters, UK). 10 µl of sample were injected at a concentration of 0.7 mg/mL. Eluent A consisted of 10 % w/v acetonitrile and 0.1 % w/v trifluoracetic acid in ultrapure water. Eluent B consisted of 0.1 % w/v trifluoracetic acid in acetonitrile. The flow rate was 0.2 mL/min. The column oven temperature was set at 75 ºC. A preheater was included before the column. A gradient of 25 to 40 % eluent B in A in 20 minutes was used. The chromatograms were integrated in Empower V3 (Waters, USA). A mass recovery of 100 % was always achieved.

4 RESULTS

A full factorial design of experiments was applied to study PPI-1 (pI=7.9). Response surface methodology was then used to study the interactions of the investigated factors. We assessed the full model and then reduced it to only the terms that were deemed statistically relevant. A curvature response was allowed by assessing the quadratic term considering also two-way interactions. The reduced model was obtained using a backward stepwise regression. The F-statistic approach was used to perform the effect test considering a value of 0.05 or less as statistically significant. These calculations were performed by the statistical software JMP® v 14.0 (SAS Institute Inc., Cary, USA). This approach was not successful to quantitatively separate the factors' effects related to the colloidal stability (e.g. degree of oligomerization, k_D, T_{agg}). This is due to an intrinsic non-linearity of PPI-1 association, which yields to very high fit errors and low accuracy and therefore poor interpretability. Hence, we discuss the investigated factors separately in sections 4.1-4.4. Differently, the apparent T_m measured by intrinsic DSF (**Table SI 2**) present a good fit with and R^2 and RSME of respectively 0.93 and 1.4. The pH presents a significant effect on the DSF profile resulting in higher apparent T_m at higher pHs, while NaCl concentration showed an almost insignificant effect in the concentration range investigated (p-value > 0.05). Nonlinear methodologies have been proved successful to predict biophysical properties of PPI-01 and other mAbs based on the amino acid composition, pH and NaCl concentration.[30]

4.1 The pH effect

The sedimentation coefficient (S) of PPI-1 between pH 5 and 7.5 at 0.1, 0.5 and 1 mg/ml (**Fig. 1(A)**) was calculated from AUC measurements. We observed an increasing amount and size of oligomers with increasing pH. A table with the weight-average Sedimentation coefficient (S_w) is reported in **Table SI 3**. S_w is reported for all the peaks and calculated across the entire distribution. The S_w is a critical parameter used to understand protein self-association.[31] AUC results correlates well with both the R_h calculated by DLS (**Fig. 1 (B)** and **1(C)**) and the R_g calculated by SAXS (**Fig. SI (4)**). DLS results also indicate a step decrease of the oligomer size at pH 8 and 9 (**Fig. 1(C)**). More information regarding SAXS results can be found in **SI 3**. All the techniques confirm the presence of monodispersed solution of the monomer at pH 5.

Physical separation of the oligomers was attempted by AF4-MALS. This technique was selected as the mobile phase can be matched to the exact formulation of the measured sample. AF4 chromatograms are shown in **Fig. SI 5**. By AF4 theory R_h was calculated from the maximum of the eluting peak. The obtained R_h values correspond to the ones measured by DLS within the experimental error (**Fig. 1 (C)**). However,

the M_w calculated from MALS yields a consistent molecular weight of around 154 kDa indicating the presence of monomer M_w. This effect is probably due to the AF4 separation process. The molecules are pushed towards the membrane during separation and then diluted before reaching the detector. Therefore, PPI-1 probably separates in its oligomeric form but rapidly equilibrates back to the monomer due to the dilution at the end of the channel.

Further, PPI-1 self-interaction was investigated by the apparent k_D (**Table SI 2**). It was not possible to differentiate the interaction effect from the oligomerization effect on the light scattering signal. This is due to the fact that the abundance of the complexes will increase with increasing solute concentration, leading to an apparant negative value of the apparent k_D.[32]

4.2 The salt effect

Formulation with high salt content always yielded the apparent size of the monomer around 5.3 nm (**Fig. 1(C)**). Titration with sodium chloride was performed and the sedimentation coefficient of PPI-1 at 1 mg/mL was analyzed by AUC at pH 6 and 6.5 (**Fig. 2, Table SI 3**). A broad distribution of oligomers was observed at zero NaCl concentration. A lower distribution of oligomers was observed at higher concentration of NaCl (**Fig. 2**, **Table SI 3**). The AUC results correlate well with other experimental techniques, which show a reduction of oligomers at increasing concentration of salt. However, at low ionic strength (<10 mM) the apparent radius of protein will increase (i.e. decreasing the sedimentation coefficient)[33] and may lead to quantitatively inaccurate interpretation of the results.

SEC-MALS yielded no elution from the column when low salt eluents were used. However, high salt eluents (i.e. PBS as described in materials and methods) yielded 99.9 % of monomer for all the formulations studied. This behavior is due to the buffer exchange over the column, which shifts the equilibrium from oligomers to monomers. Further, the salt could influence the interactions between the SEC stationary phase and PPI-1, regardless of its oligomerization state. Nonetheless, column mass recovery correlates with the formation of oligomers, as highlighted by the R_h measured by DLS (**Fig. 1 (C)**), where lower recovery (**Fig. SI 6**) is observed in formulation with higher R_h measured by DLS (**Fig.1 (C)**).

Further, we investigated the stability of PPI-1 under isothermal stress after long term storage by SEC-MALS. PPI-1 in four different formulations was stored for six months at 4, 25 and 40 °C (**Fig. 3**). Taking into consideration only soluble aggregates, the lowest aggregate content is detected at pH 6.5. The

addition of salt has a minor impact. On the other hand, at pH 5 a steep increase of aggregates is observed after 6 months of storage at 40°C. The monomer loss, which includes both soluble aggregates and the mass lost to insoluble aggregates, indicates formation of the latter (observed also by visual inspection) at pH 5. As previously mentioned the monomer loss in conditions where PPI-1 presents native self-association is possibly due to the precipitation of the oligomers (**Fig. SI 6**), which is also observed in unstressed conditions.

4.3 The temperature effect

The temperature effect on PPI-1 self-association was studied by means of light scattering experiments with temperature ramps (**Fig. 1(D)**). We observed two mechanisms of aggregation: i) irreversible non-native aggregation (i.e. pH 5) ii) reversible native disassociation with subsequent unfolding, which leads to irreversible non-native aggregation. Formulation including high salt concentration (**Fig. SI 7**) always presented non-native aggregation. We confirmed the reversibility of the first step of the second mechanism by temperature cycles between 0 and 45 °C (**Fig. 4**). The association/dissociation is fully reversible between 0 to 20 °C. Upon ramping from 25 to 45 °C a very small amount of PPI-1 of around 0.5 % appears to irreversibly aggregate in each cycle probably due to a small population of partially unfolded molecules formed with each cycle. Similarly, we confirmed the irreversibility of the second step by cycling the temperature in the range of 45 to 55 °C (**Fig. SI 8**). We noticed that PPI-1 irreversibly aggregates if the temperature reached the onset temperature of unfolding measured by nanoDSF (**Table SI 2**).

4.4 The protein concentration effect

PPI-1 formed more and larger oligomers with increasing concentration in the range of 1 to 20 mg/mL as detected by DLS (**Fig. 1(B)**), SLS (**Fig. 1(D)**), AUC (**Fig.1(A)**) and SAXS (**Fig. SI 3**). DLS indicates the formation of large particles at low concentration at pH 6.5 and 7 (**Fig.1(B-D)**) .These particles rapidly sediment during AUC experiments. Therefore, we further investigated PPI-1 at pH 6.5 without salt in diluted samples by DLS (**Fig. 5**). Three different slopes for the linear correlation between the apparent diffusion and PPI-1 concentration were observed. Between 0.1 and 0.4 mg/mL the diffusion coefficient increases linearly with concentration. From 0.4 to 2 mg/mL the diffusion coefficient shows a steep

negative linear dependency on concentration followed a more gradual decrease with concentration above 3 mg/mL.

4.5 Fab and Fc fragments studies

A fractional design of experiment was applied to PPI-1 fragments due to material limitations. We focused on solutions where oligomers were present, i.e. low ionic strength. The absence of oligomers in formulation including salt for PPI-1 fragments was confirmed by DLS and SLS. pKa based calculations of the pI of the whole mAb, its Fab and its Fc fragment, yielded 7.9, 6.2 and 8.4 respectively. Therefore, we hypothesized that the native reversible self-association may be caused by hydrophobic patches of the Fab fragment. Other low volume techniques (e.g. CG-DLS) were not successful to investigate Fab-Fab, Fab-Fc and Fc-Fc association. In fact, as previously mentioned in the case of the whole mAb, it is not possible to tell the interaction effect from the oligomerization effect on the light scattering signal. However, oligomers were observed only in the presence of the Fab fragment. To prove that the reversibility of the process is equal to the one of the whole mAb, we firstly exploited PPI-1 behavior by temperature cycling as described in section 4.3.We confirmed our hypothesis studying the whole mAb, the Fc and Fab fragments by SLS at pH 5 and 6 (**Fig. 6**). Upon a series of temperature cycles at pH 6 self-(dis)associating oligomers for both the whole mAb and its Fab fragment were observed. On the other hand, the Fc fragment was present in its monomeric form over the cycles. At pH 5 no self-association is seen. The mixtures of Fab-Fc, Fc-PPI-1 and Fab-PPI-1, were similarly investigated, however, as the Fab or PPI-1 oligomers are responsible for most of the light scattering signal, results from this experiment are similar to the one showed in **Fig. 6**. Further, Non-native irreversible aggregation starts once that $T_{m,on}$ is reached (**Fig. SI 8**). Finally, we observed a considerable difference in the retention time measured by UPLC-RP between the whole mAb, the Fc and the Fab fragment, which eluted at 2.9 mL, 2.58 mL and 3.2 mL respectively (**Fig.7**). Thus, the Fab fragment showed a rather high degree of hydrophobicity compared to the Fc fragment and the whole mAb.

5 DISCUSSION

5.1 Rationalization of PPI-1 native reversible self-association

Protein aggregation can occur through a number of distinct pathways that are not mutually exclusive. PPI-1 presents a reversible association of the native monomer that is intrinsic under certain solution conditions. In this conditions, the surface of PPI-1 in the native structure is self-complementary and

readily self-associates to form oligomers. Insulin is a typical example of therapeutic protein which forms reversible oligomers.[34] Conversely, the first step of irreversible aggregation it is due to partial unfolding of the monomer, which acts as precursor of disordered oligomers. [35–42] We carried out long term stability studies (**Fig. 3**) to differentiate these two mechanisms. We observed that PPI-1 does not form critical percentage of aggregates at room temperature or if refrigerated after six months of storage. On the other hand, high temperatures induce formation of non native aggregates at acidic pHs. It is known that acidic pHs lower the conformational stability of mAbs,[43] which most likely prompts the nonnative aggregation of PPI-1 stored at 40°C. In fact, PPI-1 was demonstrated to have a lower apparent temperature of unfolding (T_{m1}) at lower pHs (**Table SI 2**). Further, the addition of salt does not influence (at the low concentration used) the conformational stability of PPI-1. Therefore, the formulation with 10 mM histidine and 140 mM NaCl at pH 6.5 allows to both minimize the non native aggregation and eliminate PPI-1 native oligomers. The latter has been observed to induce phase separation, precipitation and high viscosity.[12,15] Several mAbs are known to have a tendency of intrinsically self-interacting, which prompts phase separation at high concentrations.[44–46] Therefore we focused our investigation into the characterization of PPI-1 native reversible association. This process is schematically summarized in **Fig. 8,** and hereafter the aim of the discussion is to rationalize this behavior. It has been suggested that self-association at low ionic strength is due to electrostatic interaction.[47] We observed for PPI-1 that the association process is weakened at low pH values (**Fig. 1**), which is due to the increasing mAb net charge. High net charge prevents short range interactions as described by the DLVO or proximity energy theory.[48,49] PPI-1 salting-in effect (**Fig1 (C) and Fig. 3**) i.e. as the ionic strength increases, protein solubility increases can be rationalized by DLVO or proximity energy theory only if a very strong dipole moment is assumed. In fact, high ionic strength depletes electrostatic interactions like charge-charge repulsion, charge-dipole and dipole-dipole attraction. PPI-1 shows, at low ionic strength, an increase of R_h and M_w with increasing pH up to 7.5 followed by a steep decrease at pH 8 (**Fig. 1(D)**). pKa based calculations of the pI of the whole mAb, its Fab and its Fc fragment, yielded respectively 7.9, 6.2 and 8.3. This supports the hypothesis of a different local surface charge behavior of PPI-1. For example, a strong self-association is detected from pH 6 (**Fig. 1, 2, 4, 6**) , which is close to the Fab pI, a milder self-association is detected at pH 8 (**Fig 1 (C)**) as the Fab is negatively charged, and no self-association at pH 5 were the Fab is positively charged (**Fig. 1, 6**) . Therefore, we digested PPI-1 to study the behavior of its fragments. We demonstrate that the native reversible self-association of PPI-1 is driven by Fab-Fab interaction (**Fig. 6**), by exploiting PPI-1 temperature dependent behavior (**Fig. 4, 6**). It has been shown that high mAb viscosity can be mediated by Fab-Fab self-association[11] and that IgG1 self-association can be driven by either the Fab or the Fc

region.[12,50] The hydrophobic aggregation-prone regions, identified by Chennmsetty et al,[51,52] are found more frequently on the Fc region than on the Fab regions. However, we observed that PPI-1 Fab fragment present a higher degree of hydrophobicity compared to the Fc fragment by UPLC-RP (**Fig. 8**). As the primary sequence of molecules studied in literature is unfortunately not available, it is impossible to compare IgG1 molecules showing pronounced self-association and identify molecular moieties on the Fab or Fc that could drive the association. Herein, we provide the primary sequence of PPI-1 to possibly increase the molecular understanding of IgG1 self-association (**SI 9**). We suggest that PPI-1 native reversible association is i) highly dominated by the Fab fragments interaction, ii) that the locus of the interaction is located on the Fab fragment, and iii) that the association is due to hydrophobic interactions. The short-range nature of the hydrophobic interaction can explain the pH dependent behavior (**Fig. 1**). Higher charge at low pH values prevents the short-range interaction from being accessible. If only the Fab is considered, with net neutral charge species at pH values close to 6, the salting-in effect (**Fig. 1, 2**) can be rationalized. For charge-neutral species many theoretical considerations were developed to explain initial salting-in of proteins.[53–55] It has been shown, that mAbs close to their pI reveal a general salting-in effect by all anions.[56] The Debye-Huckel theory, in combination with the Kirkwood´s theory expression of the dipole moments, actually predicts a salting-in effect which is consistent with the observation of protein behavior near their respective pIs.[57] This would explain the strong effect of Na^+ and Cl^- to dampen the PPI-1 native self-association (**Fig. 1, 2**). We expect Na^+ to weakly interact with the fragment surface and Cl^- could specifically bind to the protein surface. The idea of attractive electrostatic interaction is supported by salting-in behavior of KF close to its pI.[58,59] In addition, this is in agreement with the observation that a chaotropic monovalent ion binds more strongly to a net-charge neutral molecule.[60,61] Therefore, attractive electrostatic interactions may dominate at the Fab-Fab interaction site(s) at pHs near the Fab pI, where the cation and anion binding strengths with the protein surface determine the decreasing protein native self-association as the salt is increased. Further, a hydrophobic interaction supports the oligomers disassociation by increasing the temperature of PPI-1 and its Fab fragments (**Fig. 4, 6**). Hydrophobic association occurs as a result of a more ordered water structure in the proximity of nonpolar hydrocarbon groups.[62] It has been estimated that the change of entropy for protein-protein hydrophobic associations is positive.[63] This would thermodynamically support a disassociation at higher temperature as entropically driven. As expected, at increased PPI-1 concentrations an increased degree of self-association was observed (**Fig. 1(B)**). In fact, higher mAb concentration increases the entropy of mixing which will tend to decrease the activation energy required to aggregate by increasing the potential energy baseline.[49] Interestingly, PPI-1 shows the formation of large particles once a lower

concentration threshold is reached and exceeded (**Fig. 1(B), Fig. 5**), and this is only observed under conditions that prompt PPI-1 native reversible self-association. The mAbs self-association is driven by the minimization of solvent exposed hydrophobic surfaces on the Fab fragment. We hypothesize that under a critical value the mAb concentration is not enough to self-stabilize and therefore a phase separation occurs. However, further studies are necessary to properly characterize PPI-1 behaviour at very low concentration.

5.2 Lessons learned: pitfalls to study PPI-1 reversible native self-association

Batch DLS, batch SLS, SEC-MALS, AF4-MALS, CG-MALS, DLS-MALS, AUC, nanoDSF and SAXS were applied to investigate PPI-1. Due to the ubiquitous native reversible self-association of PPI-1, only the techniques capable to measure the native sample (batch SLS and DLS, AUC, SAXS) allowed t proper assessment of the size and/or amount of the reversible oligomers. On the other hand, care in the interpretation of the results is necessary if the technique applied involves the modification of either pH, Ionic strength, temperature or protein concentration, as the equilibrium of the system will be shifted. Due to the unusual behavior of PPI-01 as a function of its concentration (**Fig. 1(B)**, **Fig. 5**), pH (**Fig.1**) and salt concentration (**Fig. 1 (C), 2**), the SEC-MALS (**Fig. 3**) cannot be applied to investigate PPI-1 reversible self-association. In fact, the buffer exchange and dilution over the column impacts the mass recovery even without stress (**Fig. SI 6**). However, SEC-MALS remains a valuable tool to characterize the formation of irreversible nonnative aggregation. Other fractionation methods had similar issues, for example AF4 does not allow to properly characterize the sample due to the intense dilution over the channel (**Fig. SI 5**). Further, the uncommon behavior of PPI-1 as a the function of the concentration (**Fig. 1(C)**, **Fig. 5**) does not allow the assessment of the stoichiometry and constants of dissociation with limited amount of material (e.g. CG-MALS, AUC). This could be a limiting factor for mAbs in early stage of development, such as PPI-1. Thus, we suggest the use of nanoDSF, DLS and SLS as high-throughput technologies, and AUC as a gold-standard to characterize native reversible self-association.

6 ACKNOWLEDGMENT

This study was funded by a project part of the EU Horizon 2020 Research and Innovation program under the Marie Skłodowska-Curie grant agreement No 675074. The first author would like to thank the whole PIPPI consortium (http://www.pippi.kemi.dtu.dk) for the continuous support offered. The first author thanks Wyatt Technology staff members for their many contributions, with a special mention to Felix Gloge for the passionate discussion related to this work. The ESRF synchrotron, BM29 bioSAXS

beamline at Grenoble is acknowledged for providing beamtime for the project. PH and SM acknowledge DanSCATT for funding.

7 REFERENCES

1. Wang W, Singh S, Zeng DL, King K, Nema S. Antibody structure, instability, and formulation. *J Pharm Sci.* 2007 Jan;96(1):1-26.

2. Pavlou AK, Belsey MJ. The therapeutic antibodies market to 2008. *Eur J Pharm Biopharm.* 2005 Apr;59(3):389-96.

3. Roque AC, Lowe CR, Taipa MA. Antibodies and genetically engineered related molecules: Production and purification. *Biotechnol Prog. 2004 May-Jun;20(3):639-54*.

4. Jain, T. *et al.* Biophysical properties of the clinical-stage antibody landscape. *Proc Natl Acad Sci USA.* 2017 Jan 31;114(5):944-949.

5. Wang W. Protein aggregation and its inhibition in biopharmaceutics. *Int J Pharm.* 2005 Jan 31;289(1-2):1-30.

6. Hermeling S, Crommelin DJ, Schellekens H, Jiskoot W. Structure-immunogenicity relationships of therapeutic proteins. *Pharm Res.* 2004 Jun;21(6):897-903.

7. Braun A, Kwee L, Labow MA, Alsenz J. Protein aggregates seem to play a key role among the parameters influencing the antigenicity of interferon alpha (IFN-alpha) in normal and transgenic mice. *Pharm Res.* 1997 Oct;14(10):1472-8.

8. Telikepalli S, Shinogle HE, Thapa PS, Kim JH, Deshpande M, Jawa V, Middaugh CR, Narhi LO, Joubert MK, Volkin DB. Physical characterization and in vitro biological impact of highly aggregated antibodies separated into size-enriched populations by fluorescence-activated cell sorting. *J. Pharm. Sci.* 2015. May;104(5):1575-91.

9. Stefani M, Dobson CM. Protein aggregation and aggregate toxicity: New insights into protein folding, misfolding diseases and biological evolution. *J Mol Med (Berl). 2003* Nov;81(11):678-99.

10. Roberts CJ. Non-native protein aggregation kinetics. *Biotechnol Bioeng.* 2007 Dec 1;98(5):927-38.

11. Kanai S, Liu J, Patapoff TW, Shire SJ. Reversible Self-Association of a Concentrated Monoclonal Antibody Solution Mediated by Fab – Fab Interaction That Impacts Solution Viscosity. *J Pharm* Sci. 2008 Oct;97(10):4219-27.

12. Nishi H, Miyajima M, Wakiyama N, Kubota K, Hasegawa J, Uchiyama S, Fukui K. Fc domain

mediated self-association of an IgG1 monoclonal antibody under a low ionic strength condition. *J Biosci Bioeng.* 2011 Oct;112(4):326-32.

13. Yadav S, Sreedhara A, Kanai S, Liu J, Lien S, Lowman H, Kalonia DS, Shire SJ. Establishing a link between amino acid sequences and self-associating and viscoelastic behavior of two closely related monoclonal antibodies. *Pharm Res.* 2011 Jul;28(7):1750-64.

14. Shire SJ, Shahrokh Z, Liu J. Challenges in the development of high protein concentration formulations. *J Pharm Sci.* 2004 Jun;93(6):1390-402.

15. Liu J, Nguyen MD, Andya JD, Shire SJ. Reversible self-association increases the viscosity of a concentrated monoclonal antibody in aqueous solution. *J Pharm Sci.* 2005 Sep;94(9):1928-40.

16. Hall CG, Abraham GN. Reversible Self-Association of a Human Myeloma Protein. Thermodynamics and Relevance to Viscosity Effects and Solubility. *Biochemistry.* 1984 Oct 23;23(22):5123-9.

17. Hall CG, Abraham GN. Size, shape, and hydration of a self-associating human IgG myeloma protein: Axial asymmetry as a contributing factor in serum hyperviscosity. *Arch. Biochem. Biophys.* (1984). doi:10.1016/0003-9861(84)90453-3.

18. Lindsley, H., Teller, D., Noonan, B., Peterson, M. & Mannik, M. Hyperviscosity syndrome in multiple myeloma. A reversible, concentration-dependent aggregation of the myeloma protein. *Arch Biochem Biophys.* 1984 Sep;233(2):330-7.

19. Pope RM, Fletcher MA, Mamby A, Shapiro CM. Rheumatoid Arthritis Associated with Hyperviscosity Syndrome and Intermediate Complex Formation. *Arch Intern Med.* 1975 Feb;135(2):281-5.

20. Liu J, Andya JD, Shire SJ. A critical review of analytical ultracentrifugation and field flow fractionation methods for measuring protein aggregation. *AAPS J.* 2006 *Sep 22;8(3):E580-9.*

21. Saluja A, Badkar AV, Zeng DL, Nema S, Kalonia DS. Ultrasonic storage modulus as a novel parameter for analyzing protein-protein interactions in high protein concentration solutions: Correlation with static and dynamic light scattering measurements. *Biophys J.* 2007 Jan 1;92(1):234-44.

22. Saluja A, Badkar AV, Zeng DL, Nema S, Kalonia DS. Application of high-frequency rheology measurements for analyzing protein-protein interactions in high protein concentration solutions using a model monoclonal antibody (IgG2). *J Pharm Sci.* 2006 Sep;95(9):1967-83.

23. Philo JS1, Arakawa T. Mechanisms of protein aggregation. *Curr Pharm Biotechnol.* 2009 *Jun;10(4):348-51.*

24. Schuck P. Size-distribution analysis of macromolecules by sedimentation velocity ultracentrifugation and Lamm equation modeling. *Biophys J.* 2000 Mar;78(3):1606-19.

25. Pernot P, *et al.* N Upgraded ESRF BM29 beamline for SAXS on macromolecules in solution. *J Synchrotron Radiat.* 2013 Jul;20(Pt 4):660-4.

26. Konarev PV, Volkov VV, Sokolova AV, Koch MHJ, Svergun DI. PRIMUS: A Windows PC-based system for small-angle scattering data analysis. *J. Appl. Crystallogr.* 2003 36:1277-1282.

27. Franke D, Petoukhov MV, Konarev PV, Panjkovich A, Tuukkanen A, Mertens HDT, Kikhney AG, Hajizadeh NR, Franklin JM, Jeffries CM, Svergun DI. ATSAS 2.8 : a comprehensive data analysis suite for small-angle scattering from macromolecular solutions . *J Appl Crystallogr.* 2017 Jun 26;50(Pt 4):1212-1225.

28. Semenyuk AV, Svergun, DI. GNOM. A program package for small-angle scattering data processing. *J. Appl. Crystallogr.* 1991 24:537-540.

29. Mylonas E, Svergun DI. Accuracy of molecular mass determination of proteins in solution by small-angle X-ray scattering. *J Appl Crystallogr*. 2007 40:245-249.

30. Gentiluomo L, Roessner D, Augustijn D, Svilenov H, Kulakova A, Mahapatra S, Winter G, Streicher W, Rinnan Å, Peters GHJ, Harris P, Frieß W. Application of interpretable artificial neural networks to early monoclonal antibodies development. *Eur J Pharm Biopharm.* 2019 Aug;141:81-89.

31. Schuck P. On the analysis of protein self-association by sedimentation velocity analytical ultracentrifugation. *Anal Biochem.* 2003 Sep 1;320(1):104-24.

32. Minton AP. Recent applications of light scattering measurement in the biological and biopharmaceutical sciences. *Anal Biochem.* 2016 May 15;501:4-22.

33. Cole JL, Lary JW, P Moody T, Laue TM.. Analytical Ultracentrifugation: Sedimentation Velocity and Sedimentation Equilibrium. *Methods Cell Biol.* 2008;84:143-79.

34. Pekar AH, Frank BH. Conformation of Proinsulin. A Comparison of Insulin and Proinsulin Self-Association at Neutral pH. *Biochemistry.* 1972 Oct 24;11(22):4013-6.

35. Chi EY, Krishnan S, Randolph TW, Carpenter JF. Physical Stability of Proteins in Aqueous Solution: Mechanism and Driving Forces in Nonnative Protein Aggregation. *Pharm Res.* 2003

Sep;20(9):1325-36.

36. Dobson CM. Principles of protein folding, misfolding and aggregation. *Semin Cell Dev Biol*. 2004 Feb;15(1):3-16.

37. Fink AL. Protein aggregation: Folding aggregates, inclusion bodies and amyloid. *Fold Des.* 1998;3(1):R9-23.

38. Goers J, Permyakov SE, Permyakov EA, Uversky VN, Fink AL. Conformational prerequisites for alpha-lactalbumin fibrillation. *Biochemistry.* 2002 Oct 15;41(41):12546-51.

39. Grillo AO, Edwards KL, Kashi RS, Shipley KM, Hu L, Besman MJ, Middaugh CR. Conformational origin of the aggregation of recombinant human factor VIII. *Biochemistry.* 2001 Jan 16;40(2):586-95.

40. Khurana R, Gillespie JR, Talapatra A, Minert LJ, Ionescu-Zanetti C, Millett I, Fink AL. Partially folded intermediates as critical precursors of light chain amyloid fibrils and amorphous aggregates. *Biochemistry.* 2001 Mar 27;40(12):3525-35.

41. Linding R, Schymkowitz J, Rousseau F, Diella F, Serrano L. A comparative study of the relationship between protein structure and β-aggregation in globular and intrinsically disordered proteins. *J Mol Biol.* 2004 Sep 3;342(1):345-53.

42. Uversky VN, Fink AL. Conformational constraints for amyloid fibrillation: The importance of being unfolded. *Biochim Biophys Acta.* 2004 May 6;1698(2):131-53.

43. Sahin E, Grillo AO, Perkins MD, Roberts CJ. Comparative effects of pH and ionic strength on protein-protein interactions, unfolding, and aggregation for IgG1 antibodies. *J Pharm Sci.* 2010 Dec;99(12):4830-48.

44. Jion AI, Goh LT, Oh SK. Crystallization of IgG1 by mapping its liquid-liquid phase separation curves. *Biotechnol. Bioeng.* 2006 Dec 5;95(5):911-8.

45. Ahamed T, Esteban BN, Ottens M, van Dedem GW, van der Wielen LA, Bisschops MA, Lee A, Pham C, Thoemmes J. Phase behavior of an intact monoclonal antibody. *Biophys J.* 2007 Jul 15;93(2):610-9.

46. Dumetz AC, Chockla AM, Kaler EW, Lenhoff AM. Protein phase behavior in aqueous solutions: Crystallization, liquid-liquid phase separation, gels, and aggregates. *Biophys J.* 2008 Jan 15;94(2):570-83.

47. Nishi H, Miyajima M, Nakagami H, Noda M, Uchiyama S, Fukui K. Phase separation of an IgG1

antibody solution under a low ionic strength condition. *Pharm Res.* 2010 Jul;27(7):1348-60.

48. Israelachvili JN. Intermolecular and Surface Forces: With Applications to Colloidal and Biological Systems, second ed. *Acad. Press.* 1992.

49. Laue T. Proximity energies: A framework for understanding concentrated solutions. *J Mol Recognit. 2012 Mar;25(3):165-73.*

50. Kanai S, Liu J, Patapoff TW, Shire SJ. Reversible self-association of a concentrated monoclonal antibody solution mediated by fab-fab interaction that impacts solution viscosity. *J Pharm Sci.* 2008 Oct;97(10):4219-27.

51. Chennamsetty N, Helk B, Voynov V, Kayser V, Trout BL. Aggregation-Prone Motifs in Human Immunoglobulin G. *J Mol Biol.* 2009 Aug 14;391(2):404-13.

52. Chennamsetty N, Voynov V, Kayser V, Helk B, Trout BL. Design of therapeutic proteins with enhanced stability. *Proc Natl Acad Sci USA.* 2009 Jul 21;106(29):11937-42.

53. Baldwin RL. How Hofmeister ion interactions affect protein stability. *Biophys J.* 1996 Oct;71(4):2056-63.

54. Arakawa T, Timasheff SN. Theory of Protein Solubility. *Methods Enzymol.* 1985;114:49-77.

55. Melander W, Horváth C. Chromatography on Hydrophobic Interactions of Proteins : An Interpretation in Precipitation and of the Lyotropic Series. *Arch Biochem Biophys*. 1977 Sep;183(1):200-15.

56. Zhang L, Tan H, Fesinmeyer RM, Li C, Catrone D, Le D, Remmele RL Jr, Zhang J. Antibody solubility behavior in monovalent salt solutions reveals specific anion effects at low ionic strength. *J Pharm Sci. 2012* Mar;101(3):965-77.

57. Arakawa T, Timasheff SN. The Stabilization of Proteins By Osmolytes. *Biophys J.* 1985 Mar;47(3):411-4.

58. Robinson DR, Jencks WP. The Effect of Concentrated Salt Solutions on the Activity Coefficient of Acetyltetraglycine Ethyl Ester. *J Am Chem Soc.* 1965 Jun 5;87:2470-9.

59. Nandi PK, Robinson DR. The Effects of Salts on the Free Energies of Nonpolar Groups in Model Peptides. *J Am Chem Soc.* 1972 Feb 23;94(4):1308-15.

60. Chen X, Flores SC, Lim SM, Zhang Y, Yang T, Kherb J, Cremer PS. Specific anion effects on water structure adjacent to protein monolayers. *Langmuir*. 2010 Nov 2;26(21):16447-54.

61. Chen X, Yang T, Kataoka S, Cremer PS. Specific ion effects on interfacial water structure near macromolecules. *J Am Chem Soc.* 2007 Oct 10;129(40):12272-9.

62. Frank HS, Evans, MW. Free volume and entropy in condensed systems III. Entropy in binary liquid mixtures; Partial molal entropy in dilute solutions; Structure and thermodynamics in aqueous electrolytes. *J. Chem. Phys.* 1945 13:507–532.

63. Ross PD, Subramanian S. Thermodynamics of Protein Association Reactions : Forces Contributing to Stability. *Biochemistry.* 1981 May 26;20(11):3096-102.

8 FIGURES LEGEND

Figure 1. Selected studies on PPI-1 solution behavior. Graph A shows the AUC sedimentation velocity results at a protein concentrations of 0.1, 0.5 and 1 mg/mL . All the formulations where investigated in 10 mM His from pH 5 to 7 and the data points were depicted as shown in the legend. The same formulations and color codes are used for graph B and D. Missing data at lower concentrations are due to the formation of very large, rapidly sedimenting particles. Graph B shows the apparent Rh of PPI-1 as a function of protein concentration is shown in a logarithmic scale. Graph C shows the apparent R_h of PPI-1 at 1 mg/mL as a function of the pH. Different NaCl concentration is depicted in scale of grays as shown on the legend. Graph D shows the temperature ramp curve at 1 mg/mL measured by SLS. Similar curves for the apparent Rh are generated by DLS.

Figure 2. The effect of NaCl on sedimentation coefficient of PPI-1 by sedimentation velocity AUC. All the formulations where investigated in 10 mM His at pH 6 and 6.5, which are showed on the left and right respectively. The final concentration of NaCl is shown in different color as depicted in the legend.

Figure 3. Long term stability results. Each graph represent one of the four different formulations stored for 6 months at 4°C, 25°C and 40°C depicted in blue, red and green, respectively. The percentage of aggregates is calculated by the UV signal at 280 nm. The error bars are calculated from the analytical error. The numbers on each bar represent the calculated monomer loss corrected by the recovered mass, where one stands for complete monomer loss and zero stands for no monomer loss. This is calculated including into the calculation the initial recovered mass (i.e. before stress) divided by the calculated recovered mass.

Figure 4. An example of PPI-1 temperature cycle data generated by SLS for 1 mg/mL of PPI-1 in 10 mM His at pH 6. The figure shows two temperature cycle experiments performed between 0 and 20°C and between 25 and 45°C respectively on the left and right of the graph. 1. The Mw color based on the cycle number. The first temperature ramp is depicted in bright green while the last in bright red. At the end of each cycle PPI1 was rapidly cooled (data was not collected during the cooling phase).

Figure 5. PPI-1 Diffusion coefficient as a function of the concentration. Three linear regions are identified for PPI-1 formulated in 10 mM Histidine at pH 6. The corresponding fits and confidence intervals are shown in different colors.

Figure 6. Temperature cycles investigated by SLS of the intact mAb, Fab and Fc. Temperature cycles from 25 to 45 °C are shown for all the sample at pH 5 and 6 (10 mM His) on the left and right of the graph, respectively. The Mw ratio is calculated dividing the measured Mw by the Mw detected at 25°C. mAb, Fab and Fc are respectively depicted as shown in the legend.

Figure 7. Reverse phase chromatograms. In black, blue and red are shown respectively the results from the whole mAb, the Fc and the Fab fragments.

Figure 8. Grafical representation of PPI-1 self-association as a function of 4 factors: pH, Temperature, salt concentration and protein concentration. The graph is indicative. The red, yellow and green areas represent respectly the presence of irreversible aggregates, the presence and the absence of native oligomers.

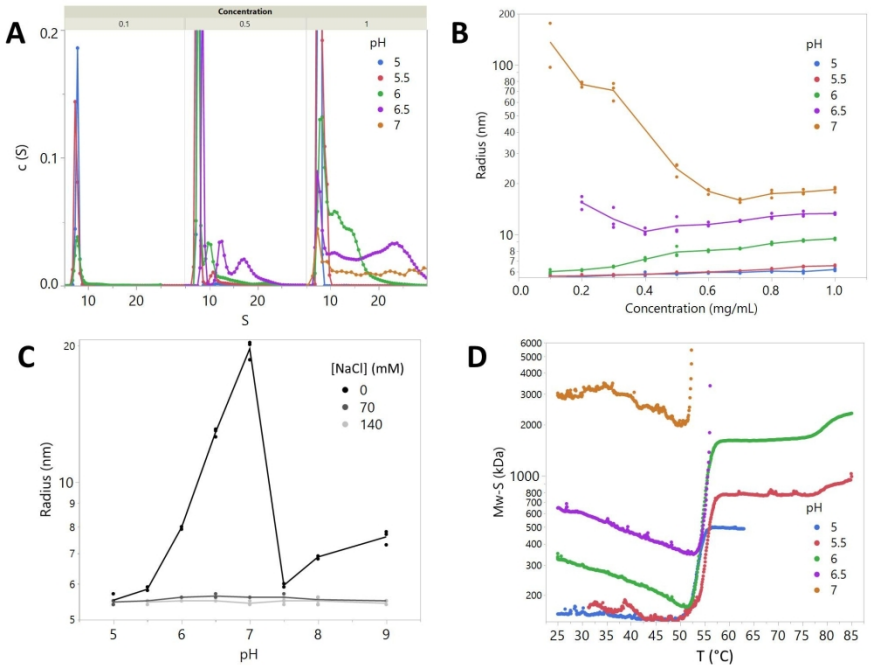

Figure 1. Selected studies on PPI-1 solution behavior. Graph A shows the AUC sedimentation velocity results at a protein concentrations of 0.1, 0.5 and 1 mg/mL . All the formulations where investigated in 10 mM His from pH 5 to 7 and the data points were depicted as shown in the legend. The same formulations and color codes are used for graph B and D. Missing data at lower concentrations are due to the formation of very large, rapidly sedimenting particles. Graph B shows the apparent Rh of PPI-1 as a function of protein concentration is shown in a logarithmic scale. Graph C shows the apparent Rh of PPI-1 at 1 mg/mL as a function of the pH. Different NaCl concentration is depicted in scale of grays as shown on the legend. Graph D shows the temperature ramp curve at 1 mg/mL measured by SLS. Similar curves for the apparent Rh are generated by DLS.

379x264mm (150 x 150 DPI)

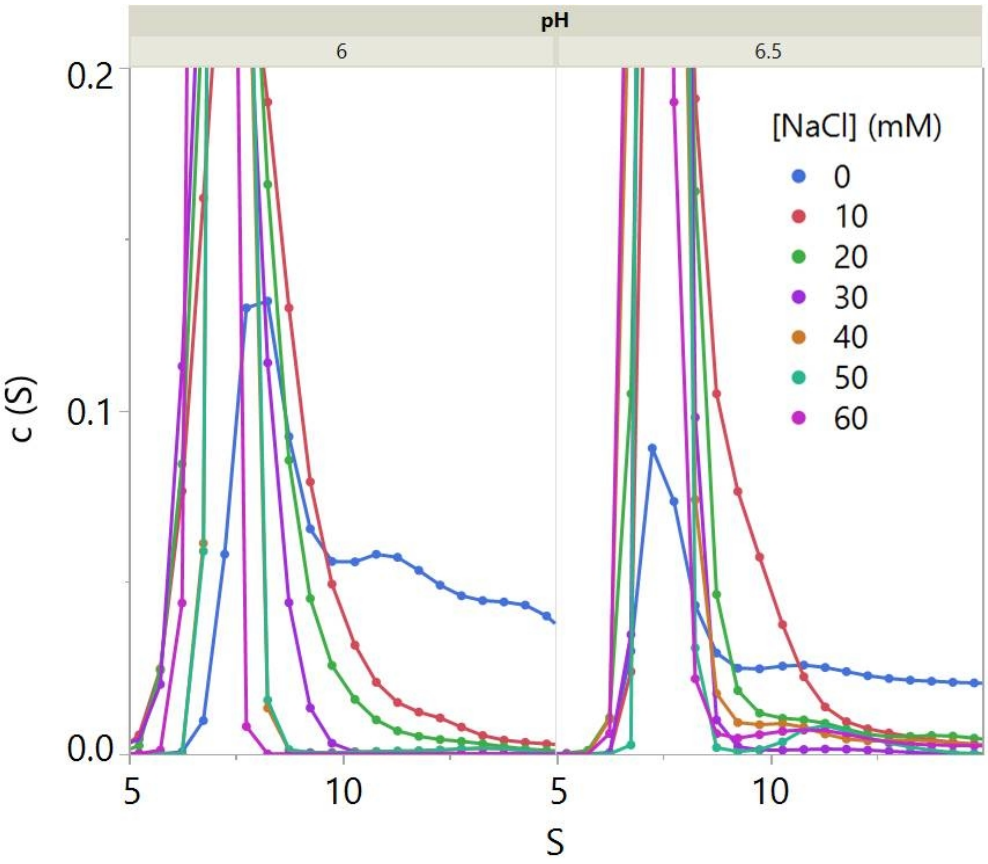

Figure 2. The effect of NaCl on sedimentation coefficient of PPI-1 by sedimentation velocity AUC. All the formulations where investigated in 10 mM His at pH 6 and 6.5, which are showed on the left and right respectively. The final concentration of NaCl is shown in different color as depicted in the legend.

146x126mm (150 x 150 DPI)

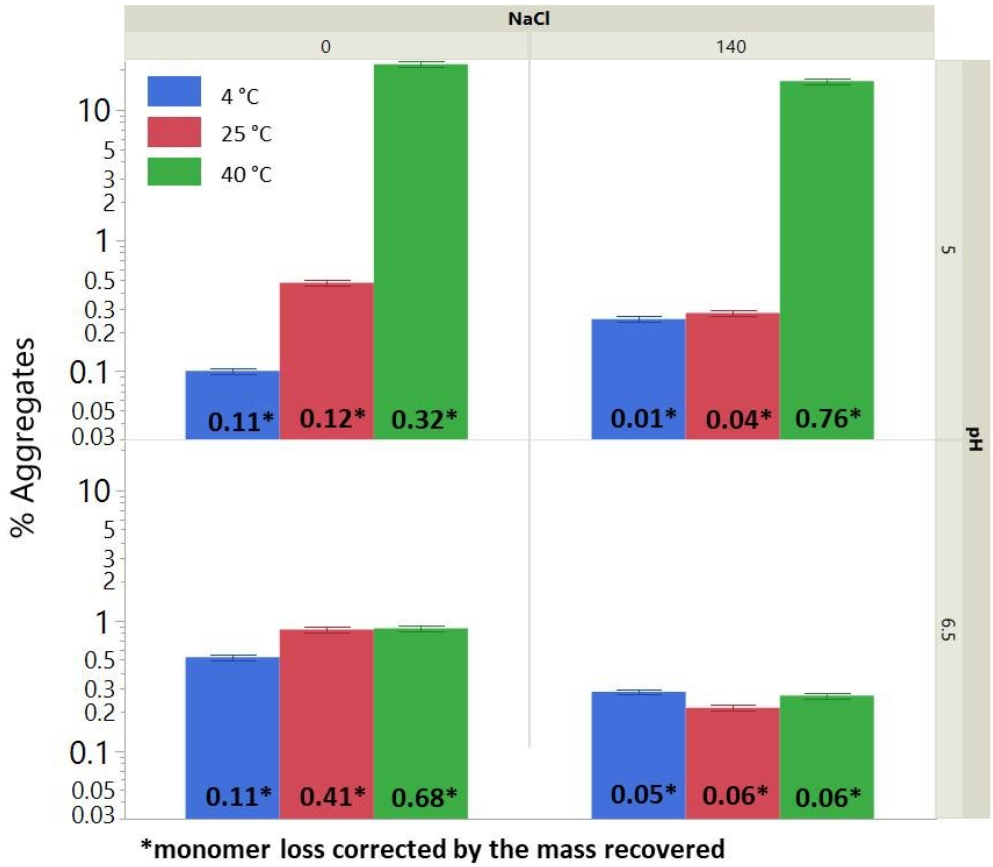

Figure 3. Long term stability results. Each graph represent one of the four different formulations stored for 6 months at 4°C, 25°C and 40°C depicted in blue, red and green, respectively. The percentage of aggregates is calculated by the UV signal at 280 nm. The error bars are calculated from the analytical error. The numbers on each bar represent the calculated monomer loss corrected by the recovered mass, where one stands for complete monomer loss and zero stands for no monomer loss. This is calculated including into the calculation the initial recovered mass (i.e. before stress) divided by the calculated recovered mass.

145x128mm (150 x 150 DPI)

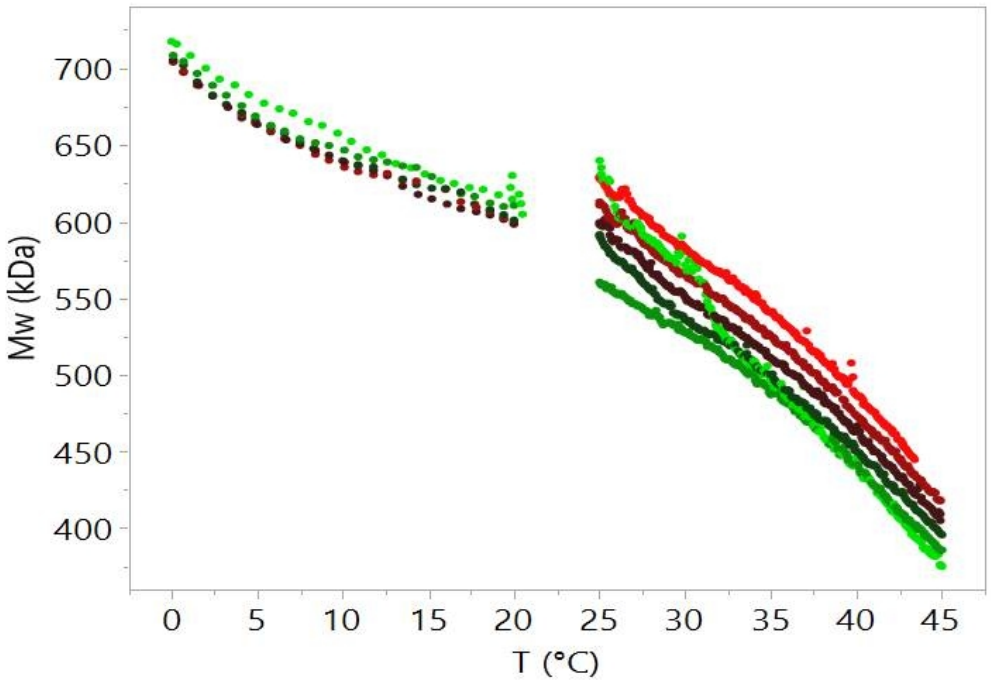

Figure 4. An example of PPI-1 temperature cycle data generated by SLS for 1 mg/mL of PPI-1 in 10 mM His at pH 6. The figure shows two temperature cycle experiments performed between 0 and 20°C and between 25 and 45°C respectively on the left and right of the graph. 1. The Mw color based on the cycle number. The first temperature ramp is depicted in bright green while the last in bright red. At the end of each cycle PPI1 was rapidly cooled (data was not collected during the coolong phase).

135x115mm (133 x 108 DPI)

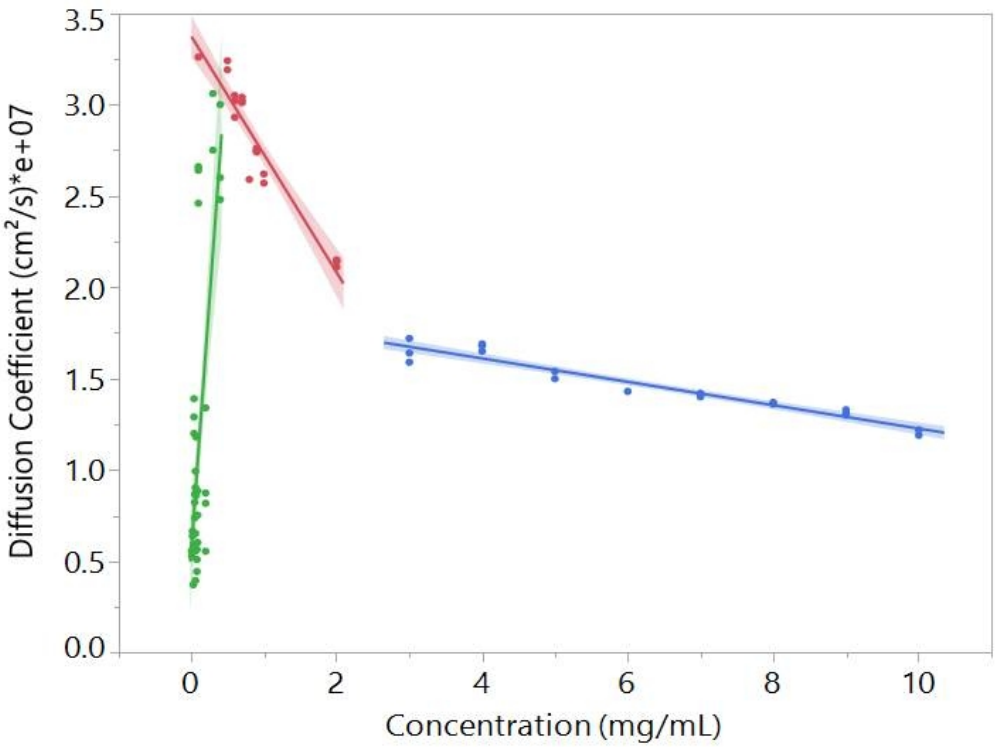

Figure 5. PPI-1 Diffusion coefficient as a function of the concentration. Three linear regions are identified for PPI-1 formulated in 10 mM Histidine at pH 6. The corresponding fits and confidence intervals are shown in different colors.

153x123mm (117 x 109 DPI)

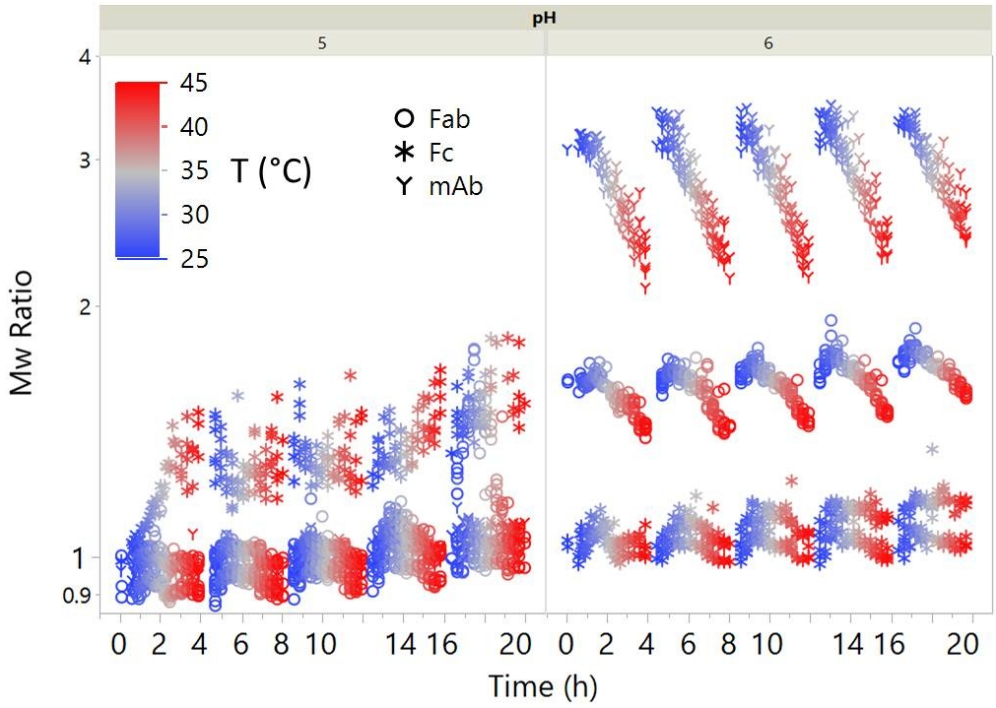

Figure 6. Temperature cycles investigated by SLS of the intact mAb, Fab and Fc. Temperature cycles from 25 to 45 °C are shown for all the sample at pH 5 and 6 (10 mM His) on the left and right of the graph, respectively. The Mw ratio is calculated dividing the measured Mw by the Mw detected at 25°C. mAb, Fab and Fc are respectively depicted as shown in the legend.

171x121mm (150 x 150 DPI)

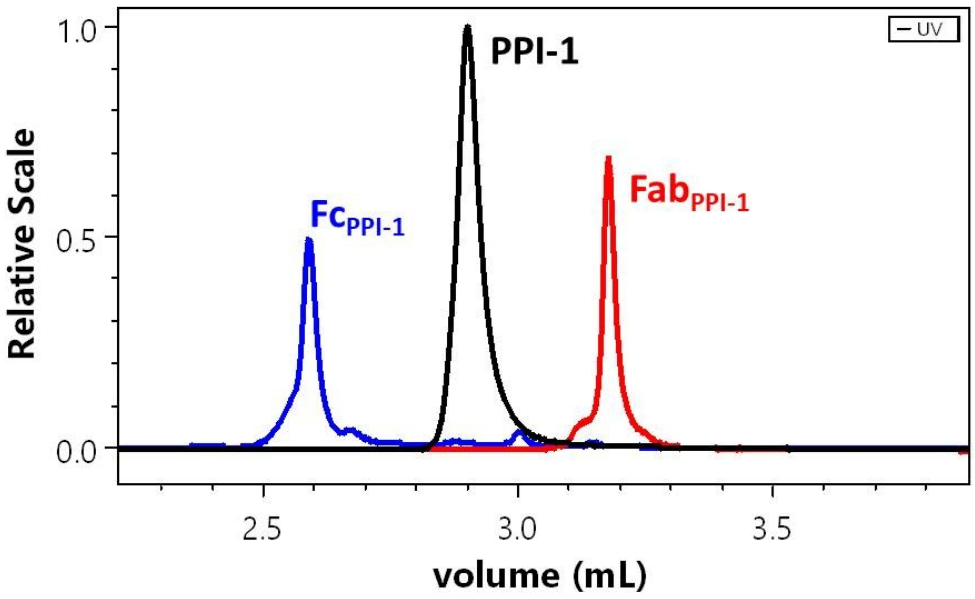

Figure 7. Reverse phase chromatograms. In black, blue and red are shown respectively the results from the whole mAb, the Fc and the Fab fragments.

152x93mm (150 x 150 DPI)

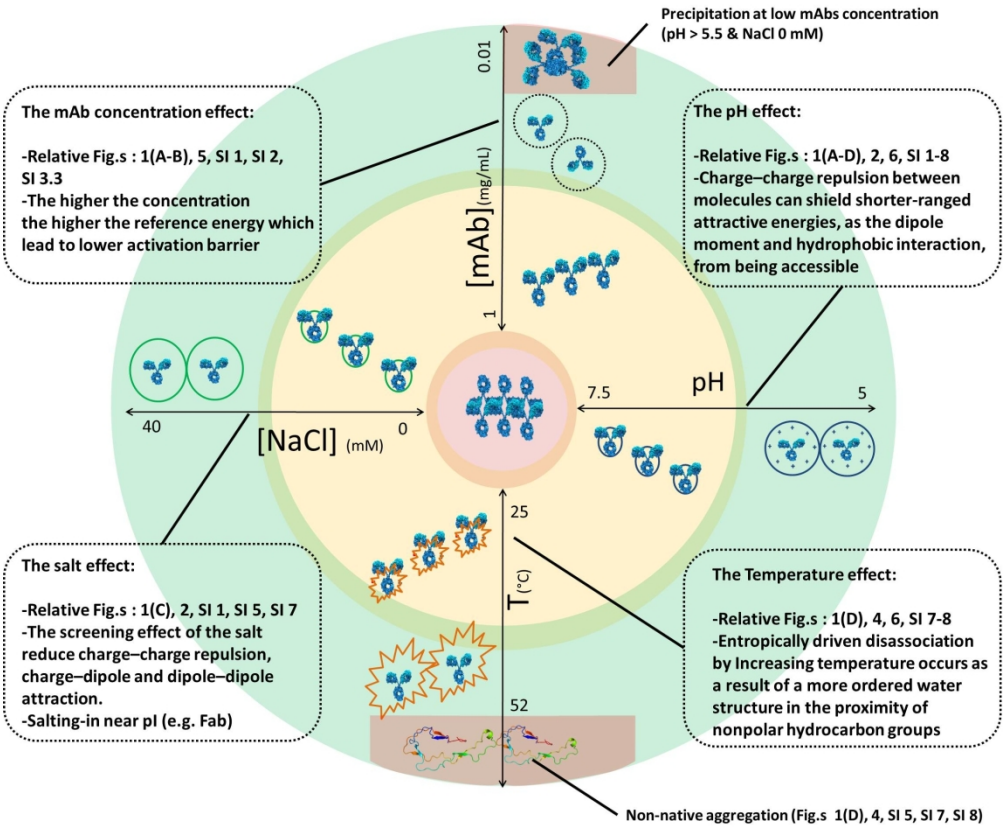

Figure 8. Grafical representation of PPI-1 self-association as a function of 4 factors: pH, Temperature, salt concentration and protein concentration. The graph is indicative. The red, yellow and green areas represent respectly the presence of irreversible aggregates, the presence and the absence of native oligomers.

382x319mm (150 x 150 DPI)

9 SUPPLEMENTARY INFORMATION

SI 1. SAXS

Table SI 1.1: Experimental set up of SAXS measurements

Instrument	ESRF, Grenoble (France), bioSAXS beamline (BM29)
Wavelength ($\AA$)	0.99
q-range ($\AA^{-1}$)	0.004 – 0.49
Sample-to-detector distance (m)	2.864
Detector	Pilatus 1M
Flux (photons/s)	2 x 10^{12}
Beam size (μm^2)	700 x 700
Sample configuration	1.8 mm quartz glass capillary
Absolute scaling method	Comparison to water in sample capillary
Normalization	To transmitted intensity by beam-stop counter
Monitoring for radiation damage	Control of un-subtracted and scaled subtracted data for systematic changes typical for radiation damage

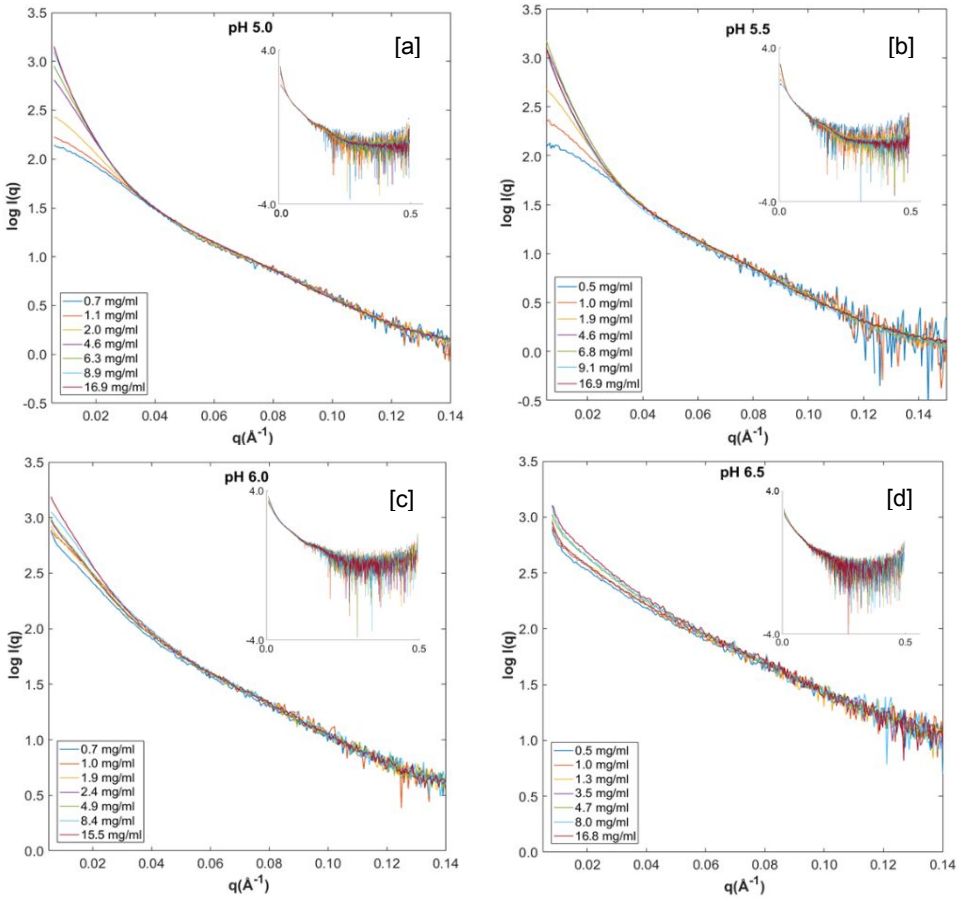

Figure SI 1.2 SAXS scattering curves: a) 10mM_Histidine_pH 5.0, b) 10mM_Histidine_pH 5.5, c) 10mM_Histidine_pH 6.0, d) 10mM_Histidine_pH 6.5. Data are shown for different PPI-1 formulation conditions with increasing concentrations.

Table SI 1.3 An overview of the samples measured by SAXS and data treatment parameters:

a) 10mM histidine pH 5.0

Protein concentration (mg/ml)	R_G (Gnom) (nm)	$I(0)/c$ (Gnom)	M_w (kDa)
0.74	6.01	0.11	156

b) 10mM histidine pH 5.5

Protein concentration (mg/ml)	R_G (Gnom) (nm)	$I(0)/c$ (Gnom)	M_w (kDa)
0.47	6.32	0.12	163

1.10	6.79	0.14	188
2.01	9.80	0.24	333
4.56	15.34	0.66	916
6.26	19.32	1.05	1451
8.94	23.24	1.74	2412
16.89	25.82	2.24	3109

1.00	8.06	0.18	249
1.93	13.55	0.44	610
4.65	19.71	1.32	1931
6.82	20.64	1.39	1828
9.11	21.51	1.42	1966
16.93	23.09	1.77	2456

c) 10mM histidine pH 6.0

Protein concentration (mg/ml)	R_G (Gnom) (nm)	$I(0)/c$ (Gnom)	M_w (kDa)
0.70	12.70	0.48	663
1.04	15.34	0.56	774
1.88	15.98	0.69	949
2.41	19.32	1.05	1451
4.92	20.24	1.58	2190
8.43	24.42	1.70	2351
15.50	26.52	2.16	2998

d) 10m histidine pH 6.5

Protein concentration (mg/ml)	R_G (Gnom) (nm)	$I(0)/c$ (Gnom)	M_w (kDa)
0.48	17.48	0.81	1119
1.01	19.74	1.26	1747
1.34	22.09	1.54	2129
3.52	23.38	1.84	2555
4.74	23.94	2.38	3298
8.03	25.48	2.50	3459
16.82	29.36	2.96	4106

Table SI 2. PPI-1 DLS and nanoDSF results.

Protein	pH	[NaCl]	k_D	T_{agg}	$T_{m,on}$	T_{m1}

			(mg/mL)	(°C)	(°C)	(°C)
PPI-1	5	0	-2.46E-02	52.69	52.12	57.44
PPI-1	5.5	0	-1.90E-02	54.28	53.43	58.84
PPI-1	6	0	-1.72E-02	55.38	54.48	60.73
PPI-1	6.5	0	-2.94E-02	56.96	54.90	62.55
PPI-1	7	0	-2.45E-02	56.8	55.29	64.62
PPI-1	7.5	0	-2.34E-02	50.82	53.78	64.31
PPI-1	8	0	-1.81E-02	49.47	56.77	69.97
PPI-1	9	0	-1.87E-02	56.5	58.98	69.99
PPI-1	5	70	-2.39E-02	45.97	49.98	54.91
PPI-1	5.5	70	-2.01E-02	50.7	52.01	57.44
PPI-1	6	70	-1.89E-02	51.98	54.61	60.30
PPI-1	6.5	70	-4.05E-02	54.41	55.64	63.14
PPI-1	7	70	-4.44E-02	51.56	56.27	63.73
PPI-1	7.5	70	-3.62E-02	55.76	56.57	64.00
PPI-1	8	70	-3.37E-02	55.48	53.60	69.93
PPI-1	9	70	2.11E-02	56.48	59.72	70.69
PPI-1	5	140	-2.01E-02	50.24	49.19	54.30
PPI-1	5.5	140	-1.74E-02	47.11	52.17	57.12
PPI-1	6	140	-2.46E-02	52.63	54.10	59.85
PPI-1	6.5	140	-1.90E-02	55.98	56.00	62.65
PPI-1	7	140	-1.72E-02	55.78	56.59	63.40
PPI-1	7.5	140	-2.94E-02	55.84	56.65	63.94
PPI-1	8	140	-2.45E-02	56.81	55.17	70.59
PPI-1	9	140	-2.34E-02	56.09	58.75	70.67

Tm fit formula: 37.102+3.875pH – (0.005[NaCl])*

Table SI 3. The effect of NaCl on the sedimentation coefficient of PPI-1 by sedimentation velocity. AUC.

The table lists the S_w from the NaCl tritation experiment showed in **Fig. 2**.

System (in 10 mM Histidine)			**Monomer**			**TOTAL AVERAGE**		
pH	NaCl (mM)	**PPI-01 (mg/mL)**	**S_w**	**Std. Dev.**	**%**	**S_w**	**Std. Dev.**	**%**
5	0	1	**7.31**	0.277	99	**7.31**	0.277	99
5	0	0.5	**7.35**	0.621	99	**7.35**	0.621	99
5	0	0.1	**7.36**	0.343	99	**7.36**	0.343	99
5.5	0	1	**7.69**	0.293	83	**7.82**	0.528	100
5.5	0	0.5	**7.52**	0.385	92	**7.75**	1.02	99
5.5	0	0.1	**7.42**	0.394	94	**10.7**	3.1	99
6	0	1	**7.8**	0.734	39	**10.77**	3.5	100
6	0	0.5	**7.85**	0.521	69	**9.28**	2.9	100
6	0	0.1	**7.4**	0.444	81	**7.89**	1.578	95
6.5	0	1	**7.78**	0.864	24	**16.82**	6.9	100
6.5	0	0.5	**7.55**	0.392	30	**11.67**	4.05	99
6.5	0	0.1	*	*	*	*	*	*
7	0	1	-	-	-	**30.1**	15.3	100
7	0	0.5	*	*	*	*	*	*
7	0	0.1	*	*	*	*	*	*
7.5	0	1	*	*	*	*	*	*
7.5	0	0.5	*	*	*	*	*	*
7.5	0	0.1	*	*	*	*	*	*
6	10	1	**7.8**	1.2	92	**8.1**	1.683	99
6	20	1	**7.5**	0.8	92	**7.73**	1.21	99
6	30	1	**7.33**	0.433	97	**7.5**	0.85	100
6	40	1	**7.3**	0.429	95	**7.3**	0.429	99
6	50	1	**7.14**	0.356	99	**7.14**	0.356	99
6	60	1	**7.23**	0.48	100	**7.23**	0.48	100
6	140	1	**6.9**	0.48	99	**6.9**	0.48	99
6.5	10	1	**8.15**	1.384	99	**8.15**	1.384	99
6.5	20	1	**7.6**	0.751	90	**7.98**	1.6	99
6.5	30	1	**7.47**	0.634	97	**7.54**	0.766	99
6.5	40	1	**7.33**	0.64	95	**7.49**	1.2	99
6.5	50	1	**7.3**	0.65	93	**7.52**	1.1	99
6.5	60	1	**7.21**	0.62	93	**7.41**	1.2	99
6.5	140	1	**7**	0.53	93	**7**	1	99

7	10	1	**7.62**	0.41	60	**9.51**	3.35	98
7	20	1	**7.43**	0.4	77	**8.23**	1.93	98
7	30	1	**7.27**	0.231	95	**7.43**	0.87	100
7	40	1	**7.3**	0.37	99	**7.3**	0.37	99
7	50	1	**7.22**	0.6	97	**7.22**	0.6	97
7	60	1	**7.1**	0.57	99	**7.1**	0.57	99
7	140	1	**6.8**	0.7	99	**6.8**	0.7	99

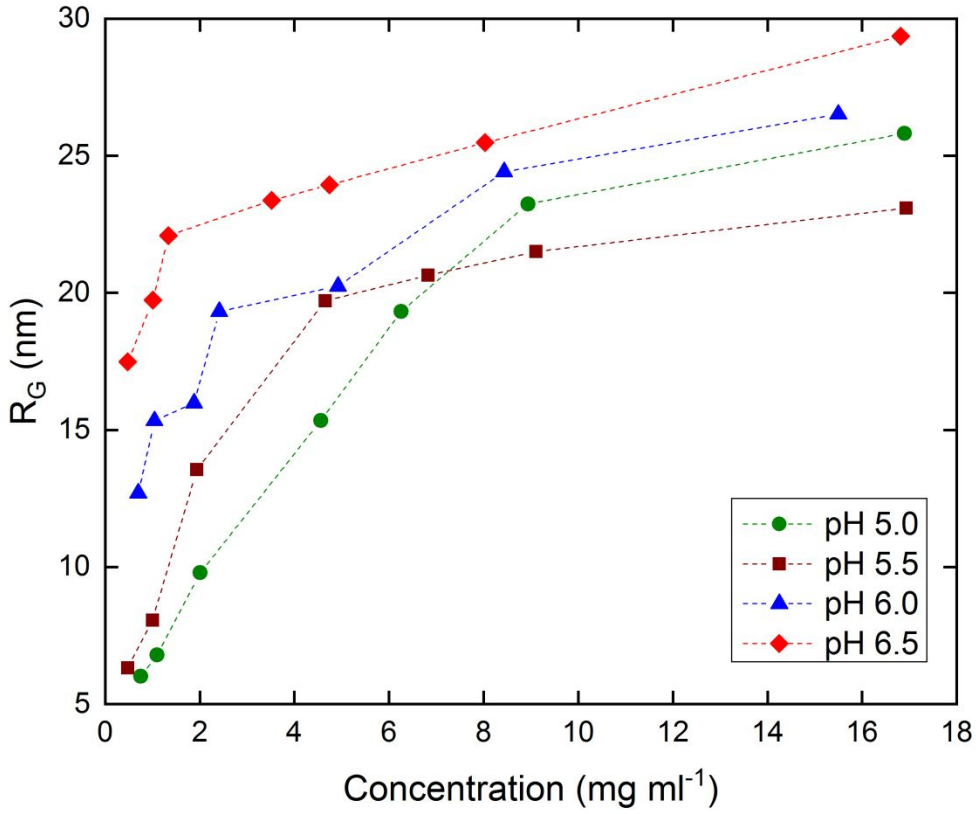

Figure SI 4 SAXS results. Four formulation (without salt) were formulated at pH 5, 5.5, 6.0 and 6.5 depicted respectively in green, brown, blue and red.

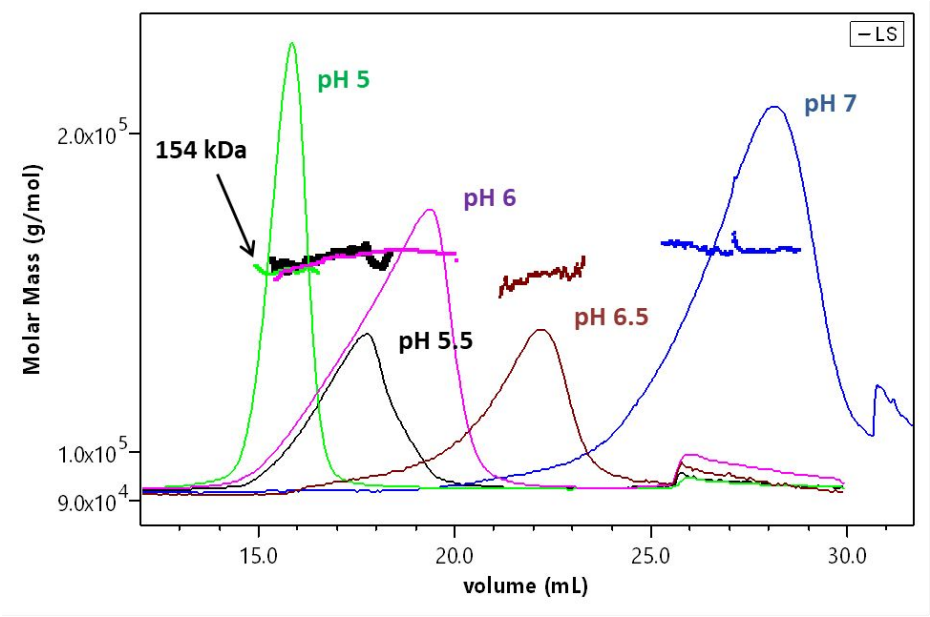

Figure SI 5. AF4-MALS chromatograms. The light scattering signal is showed for PPI-1 in different formulations. The mobile phase always match the formulation (His 10 mM for all the pHs investigated)

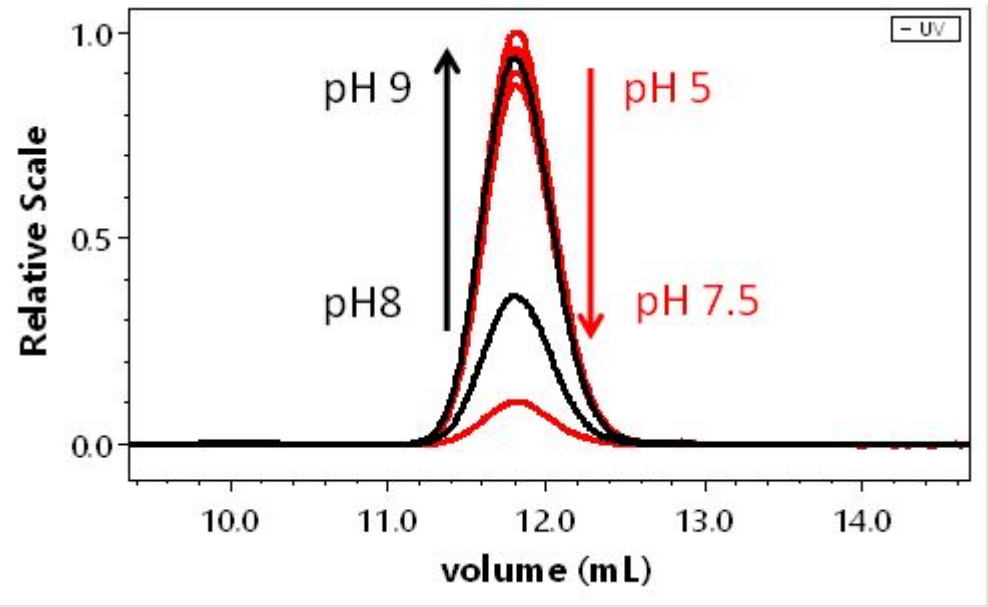

Figure SI 6. Size exclusion chromatograms. The figure include PPI-1 formulations with no salt from pH 5 to pH 9. The red and black chromatograms represent respectively a decrease of column recovery with the pH and an increase of column recovery with the pH.

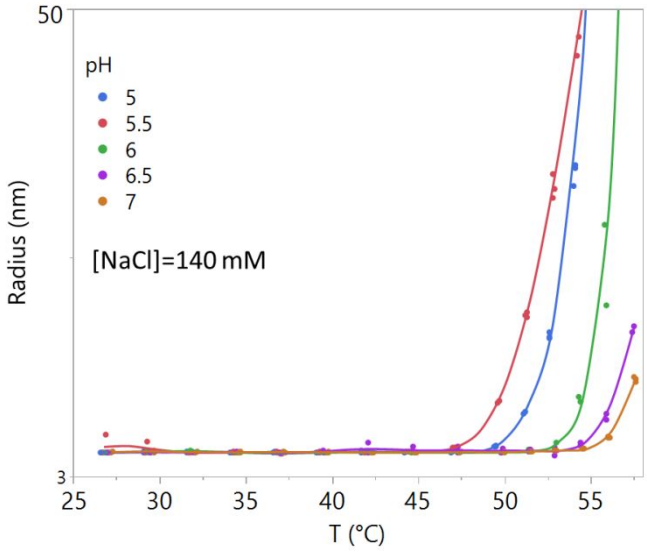

Figure SI 7. Temperature ramp curve measured by DLS. All the formulations where investigated in 10 mM His, 140 mM NaCl from pH 5 to 7 and the data points were depicted as shown in the legend.

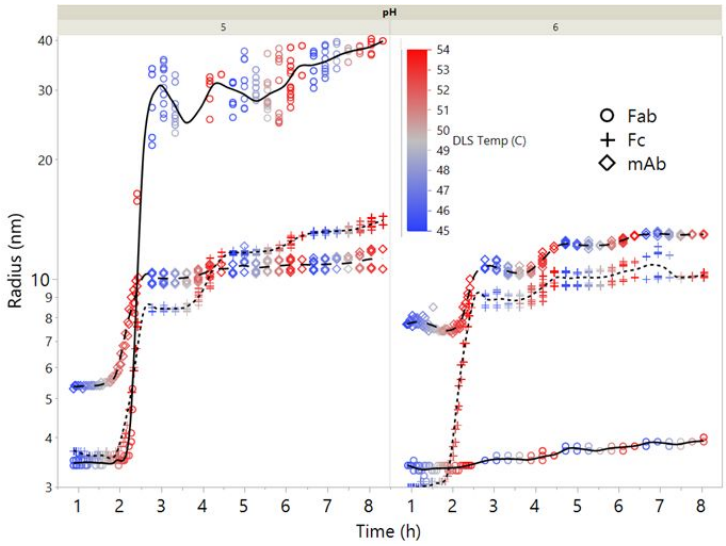

Figure SI 8. Temperature cycles investigated by DLS of the undigested mAb, Fab and Fc. Temperature cycles from 45 to 54 °C are shown for all the samples at pH 5 and 6 (10 mM His) respectively on the left and right of the graph. On the ordinates the apparent Rh is shown. mAb, Fab and Fc are respectively depicted as shown in the legend.

SI 9: PP-1 (IgG1) primary sequence.

Heavy chain
EVQLVQSGAEVKKPGATVKISCKVYGYIFTDYNIYWVRQAPGKGLEWMGLIDPDNGETFYAEKFQGRAT
MTADTSSDRAYMELSSLRFEDTAVYYCATVMGKWIKGGYDYWGRGTLVTVSSASTKGPSVFPLAPSSK
STSGGTAALGCLVKDYFPEPVTVSWNSGALTSGVHTFPAVLQSSGLYSLSSVVTVPSSSLGTQTYICNVN
HKPSNTKVDKKVEPKSCDKTHTCPPCPAPELLGGPSVFLFPPKPKDTLMISRTPEVTCVVVDVSHEDPEV
KFNWYVDGVEVHNAKTKPREEQYNSTYRVVSVLTVLHQDWLNGKEYKCKVSNKALPAPIEKTISKAKGQ
PREPQVYTLPPSRDELTKNQVSLTCLVKGFYPSDIAVEWESNGQPENNYKTTPPVLDSDGSFFLYSKLTV
DKSRWQQGNVFSCSVMHEALHNHYTQKSLSLSPGK
N-glycosylation site

Light chain
QSVLTQPPSVSGAPGQRVTISCTGSSSNIGAGYDVHWYQQLPGTAPKLLIYDNFNRPSGVPPRFSGSKS
GTSASLAITGLQAEDEADYYCQSYDSPTLTSPFGTGT
LTVLGQPKAAPSVTLFPPSSEELQANKATLVCLISDFYPGAVTVAWKADSSPVKAGVETTTPSKQSNNKY
AASSYLSLTPEQWKSHRSYSCQVTHEGSTVEKTVAPTECS